Scientific Research Publishing

Journal of Modern Physics, 2022, 13, 864-891
https://www.scirp.org/journal/jmp
ISSN Online: 2153-120X
ISSN Print: 2153-1196

Frequency Bands and Gaps of Magnetospheric Chorus Waves Generated by Resonant Beam/Plateau Electrons

Konrad Sauer[1], Huayue Chen[1,2], Eduard Dubinin[3], Quanming Lu[1,2]

[1]CAS Key Laboratory of Geoscience Environment, School of Earth and Space Sciences, University of Science and Technology of China, Hefei, China
[2]CAS Center of Excellence in Comparative Planetology, Hefei, China
[3]Max-Plnack Institute for Solar System Research, Göttingen, Germany
Email: sauer.ka@gmail.com

How to cite this paper: Sauer, K., Chen, H.Y., Dubinin, E. and Lu, Q.M. (2022) Frequency Bands and Gaps of Magnetospheric Chorus Waves Generated by Resonant Beam/Plateau Electrons. *Journal of Modern Physics*, **13**, 864-891.
https://doi.org/10.4236/jmp.2022.136050

Received: May 1, 2022
Accepted: June 21, 2022
Published: June 24, 2022

Abstract

In this paper, the modifications of the whistler dispersion characteristics are investigated which arise if resonant electrons are taken into account. The following chain of processes is emphasized: Generation of whistler waves propagating at different angles to the magnetic field and their nonlinear interaction with resonant electrons result in the appearance of modulated electron beams in the background plasma. As a result, the dispersion characteristics of waves in this new plasma might be significantly changed. By analysing the modified dispersion characteristics these changes are discussed. Supported by particle simulations and space observations, it is assumed that in the electron distribution function at the resonance velocity a plateau-like beam is formed. Because of the weakness of the beam, the term "beam/plateau population (b/p)" is used. By solving the kinetic dispersion relation of whistler waves in electron plasmas with b/p populations, the associated modifications of the whistler dispersion characteristics are presented in diagrams showing, in particular, the frequency versus propagation angle dependence of the excited waves. It is important to point out the two functions of the b/p populations. Because of the bi-directional excitation of whistler waves by temperature anisotropy, one has to distinguish between up- and downstream populations and accordingly between two b/p modes. The interaction of the beam-shifted cyclotron mode $\omega = \Omega_e + \boldsymbol{k}\cdot\boldsymbol{V_b}$ ($V_b < 0$, V_b is the b/p velocity, Ω_e: electron cyclotron frequency) with the whistler mode leads to enhanced damping at the ω-k point where they intersect. This is the origin of the frequency gap at half the electron cyclotron frequency ($\omega \sim \Omega_e/2$) for quasi-parallel waves which are driven by temperature anisotropy. Furthermore, it is shown that the up-

stream b/p electrons alone (in the absence of temperature anisotropy) can excite (very) oblique whistler waves near the resonance cone. The governing instability results from the interaction of the beam/plateau mode $\omega = \boldsymbol{k}\cdot\boldsymbol{V_b}$ ($V_b > 0$) with the whistler mode. As a further remarkable effect, another frequency gap at $\omega \sim \Omega_e/2$ in the range of large propagation angles may arise. It happens at the triple point where both b/p modes and the whistler mode intersect. Our investigation shows that the consideration of resonant electrons in form of beam/plateau populations leads to significant modifications of the spectrum of magnetospheric whistler waves which are originally driven by temperature anisotropy. Relations to recent and former space observations are discussed.

Keywords

Radiation Belts, Waves, Whistlers, Chorus

1. Introduction

Magnetospheric chorus waves have been observed over a broad spectrum reaching from about 0.1 up to 0.8 of the electron cyclotron frequency Ω_e. A remarkable feature is the appearance of a frequency gap very close to $\Omega_e/2$ which separates the spectrum in an upper and lower frequency band ([1]-[7]). Assuming electron temperature anisotropy as the sole origin of unstable waves, quasi-parallel waves close or something below $\Omega_e/2$ in warm plasmas ($\beta_e \gtrsim 0.025$, $\beta_e = 2\mu_0 n_e k T_e / B_0^2$) and oblique upper-band waves ($\theta \sim 55^\circ$) at $\omega \sim 0.6\Omega_e$ for $\beta_e \lesssim 0.025$ can theoretically be explained, (see e.g. [8] [9] [10]). However, the frequency gap and high occurrence of very oblique lower band chorus waves with $\theta \gtrsim 60^\circ$ remain, among others, a topic of current debate.

Several explanations have been proposed for the banded emissions. Either they are based on the separate generation of each band taking into account distinct anisotropic electron components which provide the source of restricted instabilities on both sides of the frequency gap, as described by [8] and [9], or a mechanism is considered which causes selective damping around $\Omega_e/2$. The studies by [11] [12] are representative for the last case. They argue that the gap is formed if the waves with a slightly oblique normal angle propagate away from the equator. Then, the associated nonlinear damping leads to a separation into a lower- and upper-frequency band around $\Omega_e/2$.

A new approach to the interpretation of the gap opened up by the investigation by [13], who showed that the self-generated deformation of the distribution function by wave-particle interaction may significantly modify the propagation properties of the driving whistler waves. In this way, the frequency-selective reduction of the growth rate leads to the gap at half the electron cyclotron frequency. The situation is similar in the recent work by [14], in which the cause of two-band chorus was investigated using 1D PIC simulations in comparison with

in-situ observations. They showed that the electron distribution function is immediately changed via Landau resonance, by which the initial unstable whistler waves split in frequency into a lower and an upper band. In [14] was argued that the resulting gap is caused by local suppression of the temperature anisotropy at medium energies.

A different concept to explain the physical nature of the frequency gap was presented by [10]. It is based on the effects of mode coupling and splitting which occur if different modes cross each other in the ω-k space. Such phenomena are known from several situations, e.g. in proton plasmas with minor abundances which lead to additional (minor ion) cyclotron waves associated with mode splitting and frequency gaps at the crossing points ([15] [16]), or the coupling between Langmuir and electromagnetic waves at oblique propagation ([17] [18] [19] [20] [21]). Similar kinds of effects may arise in the case of whistler waves at oblique propagation if the self-consistent deformation of the electron distribution function by the field-aligned electric field is considered. From particle (PIC) simulations ([22] [23] [24] [25]), as mentioned already, and *in-situ* space measurements ([26] [27] [28] [29] [30]) it is known that this interaction manifests itself in the formation of a particle group, which appears in the distribution function as a beam/plateau-like structure. As a consequence, the question arises as to what effects these resonant particles (similar to a minor component in other cases) mean for wave propagation in the frequency range of whistler waves. Based on statistical analysis of Van Allen Probe measurements, Authors in [31] were the first to show that the beam/plateau electron populations, which are formed due to resonance effects of lower-band oblique waves, can suppress the generation of parallel propagating whistler waves.

One has further to point out in the beginning that one generally has to distinguish between two beam/plateau (b/p) populations, one upstream and the other in a downstream direction with respect to the considered whistler wave. This has to do with the wave excitation through temperature anisotropy by which normally waves in both directions are driven and thus generate resonant electrons up- and downstream. These two b/p populations in turn have different effects on the whistler wave considered to travel in the positive direction. If one asks about the associated wave modes that can interact with this wave, then for the upstream electrons with the velocity V_b (>0) the beam mode $\omega = k \cdot V_b$ comes into consideration. For the downstream population, on the other side, the cyclotron mode $\omega = \Omega_e + k \cdot V_b$ ($V_b < 0$) takes on this role. In this way, the two b/p populations have very different effects on the propagation properties of the primary whistler wave. In short, it can be said: i) Using beam instability, the upstream b/p electrons can generate whistler waves outside the original frequency range. ii) The cyclotron mode associated with the downstream b/p population leads to selective damping and thus ultimately to gap formation at $\Omega_e/2$.

In recent papers ([24] [25] [32]) PIC simulations together with dispersion analysis have been used to study some of the described effects for the case of qu-

asi-parallel waves. Our approach, to split the self-consistent non-linear process of wave-particle interaction into two steps using linear theory, contains no restrictions with respect to the wave propagation angle. First, the excitation of whistler waves by temperature anisotropy is analyzed determining the phase velocity and the growth rate of the unstable waves. The decisive factor is the electron plasma beta ($\beta_e = 2\mu_0 n_e kT_e / B_0^2$) which determines the propagation properties of the whistler waves. According to the work in [9] [10] [23] [33] there is a critical value β_{cr}~0.025 which separates two regimes of propagation. For $\beta_e < \beta_{cr}$ the frequency of the unstable waves is ω~0.65Ω_e at a propagation angle of θ~50˚. The phase velocity of these waves (parallel to the magnetic field) varies with β_e as $V_{ph\|} / V_{Ae} \sim 2.8\beta_e^{1/2}$. Above the critical value ($\beta_e > \beta_{cr}$) the unstable waves propagate parallel to the magnetic field and its phase velocity remains nearly independent of β_e at $V_{ph\|} / V_{Ae}$~0.5.

In the second step, the modification of the distribution function due to resonance electrons is simulated by adding a beam/plateau (b/p) population in the parallel direction to the Maxwellian distribution. Hereby, the b/p velocity (V_b) is set equal to the previously calculated phase speed. The desired shape of the b/p distribution is modeled by the superposition of shifted Maxwellians in a narrow velocity range extending up to V_b. With such a combination of Maxwell and beam/plateau distributions, the propagation properties of whistler waves are analyzed within the framework of kinetic dispersion theory. In particular, it is shown that unstable waves can be generated by the beam/plateau electrons alone, even without temperature anisotropy. This situation can be important for wave excitation after the original instability due to temperature relaxation has subsided.

Altogether, the most essential results of the dispersion analysis including resonant b/p populations are the following: The interaction of the beam-shifted cyclotron mode $\omega = \Omega_e + k \cdot V_b$ ($k > 0$, $V_b < 0$) with the whistler mode leads to enhanced damping at the ω-k point where they intersect. This is the origin of the frequency gap at half the electron cyclotron frequency (ω~Ω_e/2) for quasi-parallel waves driven by temperature anisotropy. It is shown that (in the absence of temperature anisotropy) the upstream b/p electrons alone can excite oblique whistler waves near the resonance cone. This is caused by the interaction of the beam/plateau mode $\omega = k \cdot V_b$ ($V_b > 0$) with the whistler mode. At the simultaneous presence of the beam-shifted cyclotron mode $\omega = \Omega_e + k \cdot V_b$ ($V_b < 0$) a gap at Ω_e/2 can be formed also by oblique waves. It happens at the triple point where both b/p modes and the whistler mode intersect. Further, it is suggested that the beam mode may also contribute to the generation of harmonic waves, as known from electrostatic Langmuir waves.

The paper is organized as follows: Preliminary considerations on beam-whistler interaction distinguishing between the effects of up- and downstream b/p populations are presented in Section 2. In Section 3, kinetic dispersion analysis is carried out to investigate the whistler wave excitation due to temperature anisotropy at the presence of (minor) beam/plateau populations. The approach is split in

two parts. In 3.1, the gap formation by downstream beam/plateau population is demonstrated separately. Wave generation owing to resonant electrons and the combined action of both up- and downstream b/p populations are analyzed in Section 3.2 using $\beta_e = 0.1$. Three more examples ($\beta_e = 0.01, 0.2, 0.4$) representing cold and warm electron plasmas are treated in Section 4. Finally, the main features of magnetospheric chorus waves in the light of our investigations are discussed.

2. Preliminary Considerations on Beam-Whistler Interaction

In the following, some preliminary considerations are presented, which should make it easier to work out the fundamental concern of the kinetic investigations in Section 3 on the excitation of whistler waves by resonant beam/plateau electrons. In a fluid description, the distribution of the resonant electrons can be described by the beam speed (in both directions) $\pm V_b$, and the beam density n_b. In a water bag model, the thermal beam velocity V_{Tb} is added. These beams are generally associated with two wave modes that can interact with the whistler wave in the positive direction. This is the beam mode $\omega = k \cdot V_b$ (with $V_b > 0$) and beam-cyclotron mode $\omega = \Omega_e + k \cdot V_b$ ($V_b < 0$). Hereby, one has to be in mind that the beam speed is determined by the phase speed of the unstable waves and thus by the plasma beta of the anisotropic electron component, β_e. This means, the beam speed is $V_b/V_{Ae} \sim 2.8\beta_e^{1/2}$ for $\beta_e < 0.025$ and $V_b/V_{Ae} \sim 0.5$ for $\beta_e > 0.025$. The effects of beam-whistler interaction that are important for our later considerations are discussed below.

2.1. Mode Splitting by the Beam-Cyclotron Mode

As described in earlier work [10], the interaction of the beam-cyclotron mode $\omega = \Omega_e + k \cdot V_b$ ($V_b < 0$) with the whistler wave is of decisive importance for the formation of the frequency gap. The basic effect is the mode splitting, combined with the existence of a "forbidden" zone, which occurs in the frequency and wave number range where both modes cross, see also [34]. Similar splits are known from other wave modes, e.g. the ion-cyclotron waves in proton plasmas with small admixtures due to heavy ions ([15] [16]). If due to kinetic effects the modes merge, enhanced damping generally remains as a characteristic signature of the ongoing interaction. Examples of mode splitting using the fluid approach of cold plasmas are shown in **Figure 1(a)** and **Figure 1(b)** for two beam velocities and propagation angles. As seen there, the interaction of the beam-cyclotron mode $\omega = \Omega_e + k \cdot V_b$ ($V_b < 0$) with the whistler wave leads to mode splitting around the point of intersection. No wave propagation exists in the resulting frequency gap whose width increases with increasing beam density. The intersection point of both modes can easily be calculated. Using the approximated whistler dispersion relation $x^2 = y/(\cos\theta - y)$ with $x = kc/\omega_e$, $y = \omega/\Omega_e$ and $U_b = V_b/V_{Ae}$ (V_{Ae} is the electron Alfven velocity, $V_{Ae} = c.\Omega_e/\omega_e$, ω_e: electron plasma frequency), the wave number of the intersection point is obtained as solution of the third-order equation

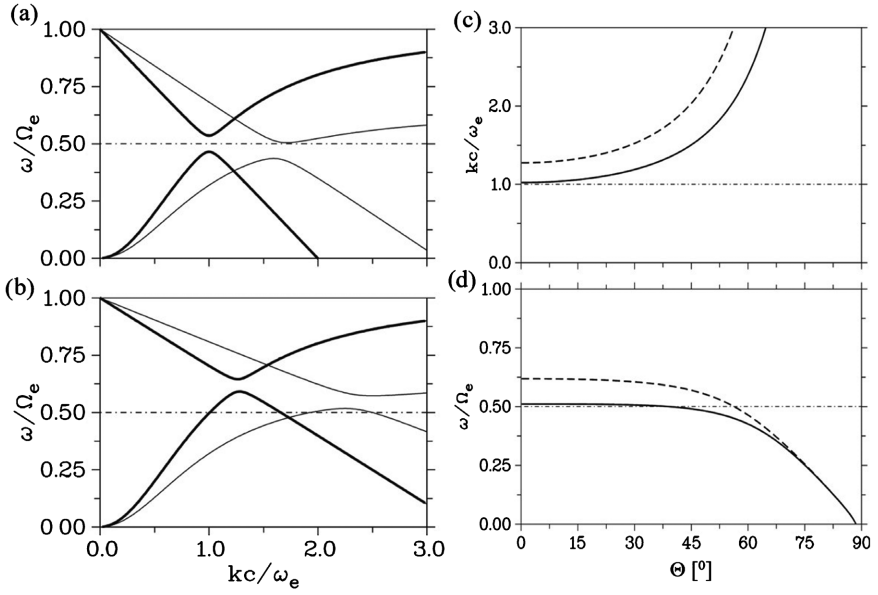

Figure 1. Mode splitting at crossing of the beam-cyclotron mode $\omega = \Omega_e + \boldsymbol{k}\cdot\boldsymbol{V_b}$ ($V_b < 0$) with the whistler mode (cold fluid theory, beam density $n_b/n_e = 0.001$): (a) $V_b/V_{Ae} = 0.5$, $\theta = 20^\circ$—solid curve, $\theta = 50^\circ$—thin curve; (b) $V_b/V_{Ae} = 0.3$, $\theta = 20^\circ$—solid curve, $\theta = 50^\circ$—thin curve. The coordinates of the intersection point (kc/ω_e, ω/Ω_e) are shown in c) and d), respectively, versus the propagation angle θ for two beam velocities: $V_b/V_{Ae} = -0.5$—solid curves, $V_b/V_{Ae} = -0.3$—dashed curves. Panels (c) and (d) represent the coordinates of the intersection point (kc/ω_e, ω/Ω_e) versus the propagation angle θ for two beam velocities: $V_b/V_{Ae} = -0.5$—solid curve; $V_b/V_{Ae} = -0.3$—dashed curve. Having in mind the occuring mode splitting along the solid curve in **Figure 1(c)**, a frequency gap around $\omega = \Omega_e/2$ can be expected if in warm plasmas ($\beta_w \gtrsim 0.025$, $V_{ph} \sim 0.5\,V_{Ae}$) quasi-parallel waves are driven by temperature anisotropy. That will subsequently be shown in Section 3.1 by means of kinetic dispersion theory.

$$U_b \cos\theta x^3 + (\cos\theta - 1)x^2 + U_b \cos\theta - 1 = 0 \tag{1}$$

In **Figure 1(c)** and **Figure 1(d)**, the coordinates of the intersection point are shown for two beam velocities.

2.2. Instability by (Upstream) Beam-Whistler Interaction

The excitation of whistler waves by electron beams has been studied in laboratory [35], and space ([36] [37]), followed by numerous analytical and numerical investigations (e.g. [38] [39] [40]). In the following, the arising beam instability itself is not of interest, but only the frequency and wave number at which maximum instability may occur. It is assumed that this happened at the $\omega - k$ points where the beam mode $\omega = k\cdot V_b$ and the whistler mode cross each other. Using, as before, the approximated whistler dispersion relation $x^2 = y/(\cos\theta - y)$ with $x = kc/\omega_e$, $y = \omega/\Omega_e$ and $U_b = V_b/V_{Ae}$, the two cutting points between the beam mode $\omega = k\cdot V_b$ ($k > 0$, $V_b > 0$) and the whistler mode are obtained by simple analytics as

$$x_\pm = \frac{1}{2U_b}\left[1 \pm \left\{1 - (2U_b)^2\right\}^{1/2}\right] \tag{2}$$

Accordingly, the frequency of the lower (−) and upper (+) beam instability

versus the propagation angle θ is given by

$$\omega_{\pm} = 0.5\Omega_e A_{\pm} \cos\theta \tag{3}$$

$$A_{\pm} = 1 \pm \left\{1 - \left(2U_b\right)^2\right\}^{1/2} \tag{4}$$

As seen in Figure 2(a) ($\theta = 50^\circ$) and Figure 2(b) ($\theta = 20^\circ$) the beam mode intersects the whistler mode at two points. The dependence of the corresponding wave number and frequency versus θ for two beam velocities V_b ($0.3\,V_{Ae}$, $0.45\,V_{Ae}$) is shown in Figure 2(c) and Figure 2(d), respectively. Considering the upper beam instability for warm electron plasma with $V_b \sim 0.5\,V_{Ae}$ ($U_b \sim 0.5$) one gets $A_+ \sim 1$ and thus $\omega_+ \sim 0.5\Omega_e \cos\theta$. That means the frequency follows almost the Gendrin angle. In the case of cold electrons with $V_b/V_{Ae} \ll 0.5$, the frequency would follow the resonance cone angle, *i.e.* $A_+ \sim 2$.

2.3. Gap Formation at $\Omega_e/2$ Involving Both Beam Modes

The main aim of this subsection is to illustrate how the whistler wave activity is decisively influenced by the simultaneous interaction of both beam modes. One has to have in mind how the individual beam mode interacts with the whistler wave: The beam mode $\omega = k \cdot V_b$ ($V_b > 0$) is responsible for the beam instability, the beam-cyclotron mode $\omega = \Omega_e + k \cdot V_b$ ($V_b < 0$) causes mode splitting and increased damping, respectively, in the interaction area. Our suggestion is: The interaction of both effects is the cause of the gap formation at $\omega = \Omega_e/2$. As first step, the intersection of both beam modes is considered. From $y = xU_b\cos\theta$ and $y = 1 - xU_b\cos\theta$ one gets immediately: $x = 0.5/(U\cos\theta)$ and $y = 0.5$; that means,

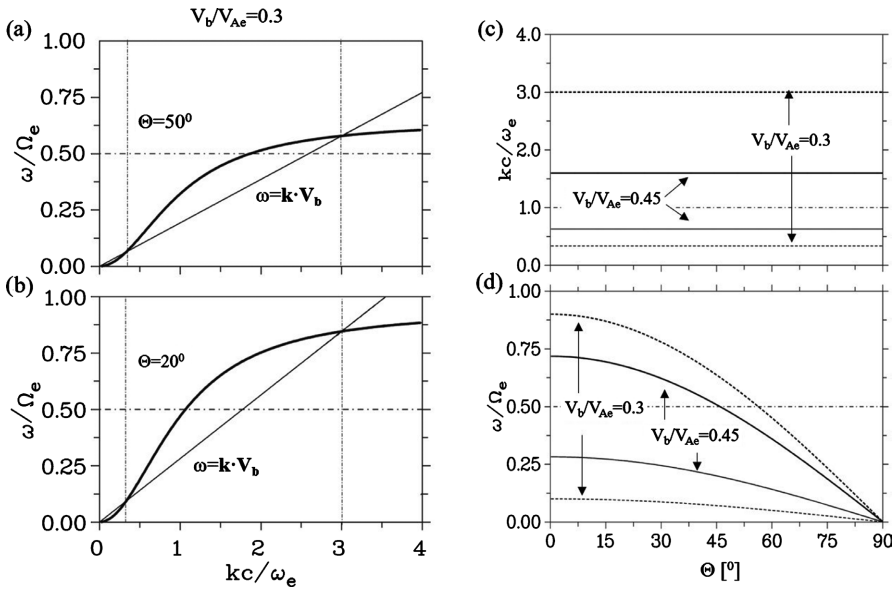

Figure 2. Intersection of the beam mode $\omega = \boldsymbol{k \cdot V_b}$ ($V_b = 0.3\,V_{Ae}$) with the whistler mode for two propagation angles: (a) $\theta = 50^\circ$, (b) $\theta = 20^\circ$. The beam mode intersects the whistler mode in two points causing the lower and upper beam instability. The coordinates of these points (kc/ω_e, ω/Ω_e) versus θ are shown in (c) and (d), respectively, for two beam velocities ($V_b/V_{Ae} = 0.3, 0.45$).

both modes always intersect at $\omega = \Omega_e/2$. Inserting the coordinates of this point into the whistler dispersion relation $x^2 = y/(\cos\theta - y)$, the simple relation between the (normalized) beam velocity U_b and the propagation angle θ results: $U_b = 0.5\,(2\cos\theta - 1)^{1/2}/\cos\theta$. These relationships are illustrated in **Figure 3**.

From **Figure 3(d)** one may conclude that for beam velocities $V_b \sim \pm 0.5\,V_{Ae}$ the frequency gap at $\omega = \Omega_e/2$ will be formed by quasi-parallel waves. In case of $V_b \lesssim 0.3\,V_{Ae}$, on the other side, mainly waves with $\theta \sim 60^\circ$ are involved. For the illustration of both cases, fluid dispersion analysis as described in [40] has been applied. The beams are described by water-bag distributions in order to include thermal effects. Results are shown in **Figure 4** for the parameters marked in **Figure 3(d)** by stars and full rectangles: $\theta = 20^\circ$, $V_b/V_{Ae} = \pm 0.49$ in (a, b), $\theta = 52^\circ$, $V_b/V_{Ae} = \pm 0.38$ in (c, d). It is noteworthy that the essential effects of the interaction, which are discussed in more detail below in the context of the kinetic theory, are already contained in the fluid approach: These are: 1) Two areas of beam instability with maxima at the intersections of the beam mode $\omega = \boldsymbol{k}\cdot\boldsymbol{V_b}$ ($V_b > 0$) with the whistler wave and 2) the formation of the frequency gap at the frequency $\omega = \Omega_e/2$, where the beam-cyclotron mode $\omega = \Omega_e + \boldsymbol{k}\cdot\boldsymbol{V_b}$ ($V_b < 0$) intersects the whistler mode.

3. Wave Excitation and Gap Formation by Beam/Plateau Population-Kinetic Approach

After the preliminary considerations on beam/whistler interaction in Section 2, kinetic dispersion theory is used to investigate how the whistler wave dispersion

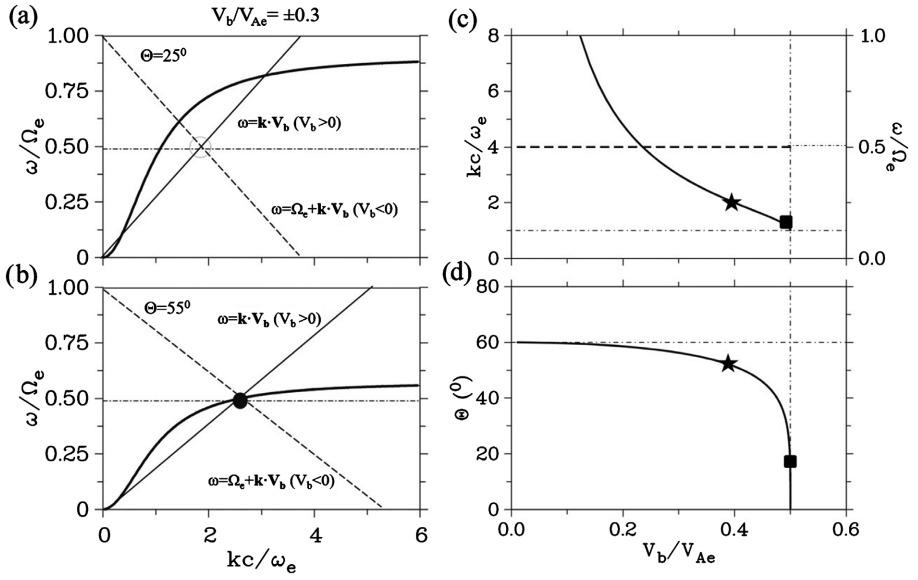

Figure 3. Intersection of both beam modes ($\omega = \boldsymbol{k}\cdot\boldsymbol{V_b}$, $V_b = 0.3\,V_{Ae}$; $\omega = \Omega_e + \boldsymbol{k}\cdot\boldsymbol{V_b}$, $V_b = -0.3\,V_{Ae}$) with the whistler mode for two propagation angles: (a) $\theta = 25^\circ$, (b) $\theta = 55^\circ$. In panel b) all three modes intersect in one point. In panels (c) and (d) the coordinates of this triple point (kc/ω_e: solid curve; $\omega/\Omega_e = 0.5$: dashed line) and the associated propagation angle θ, respectively, versus the beam velocity V_b are shown. For the conditions marked by stars and full rectangles, gap formation is presented in **Figure 4**.

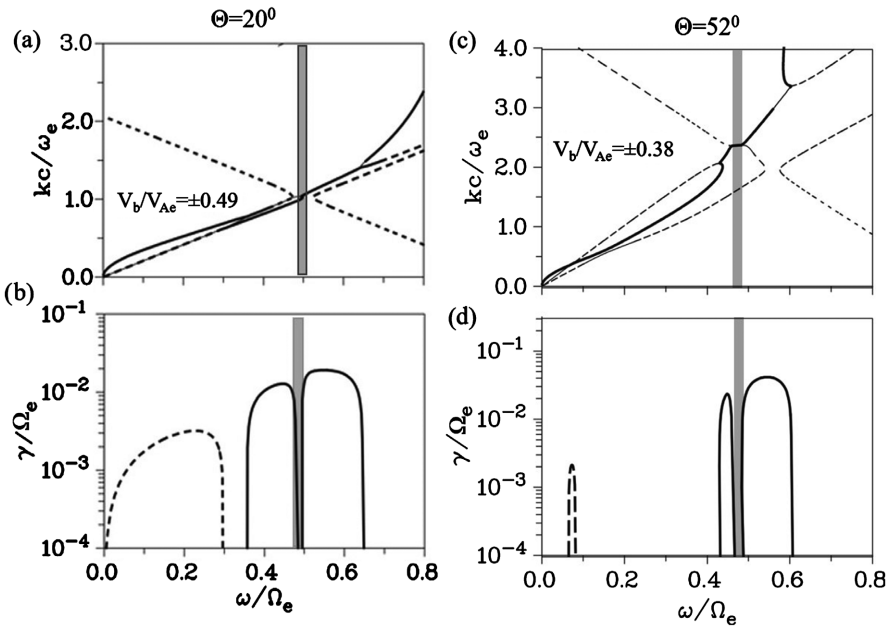

Figure 4. Gap formation involving both beam modes for the two conditions marked in **Figure 3(d)** by the star ($\theta = 20^\circ$, $V_b/V_{Ae} = \pm 0.49$) and the full rectangle ($\theta = 52^\circ$, $V_b/V_{Ae} = \pm 0.38$). The wave number kc/ω_e in (a), (c) and the growth rate γ/Ω_e of beam instability in (b), (d) versus frequency ω/Ω_e are shown. As seen in the lower two panels, a frequency gap very close to $\omega = \Omega_e/2$ is formed in both cases. The dashed curves in panels (b) and (d) represent the lower beam instability, see also **Figure 2(a)**, **Figure 2(b)**. The dispersion analysis is based on the fluid approach as described in [40] with a warm (water-bag) beam. A beam density of $n_b/n_e = 0.001$ (a), (b) and $n_b/n_e = 0.01$ (c), (d) has been taken.

is influenced by the up- and downstram beam/plateau populations which are assumed to be formed due to Landau resonance. Thus, temperature anisotropy is the primary driver of unstable whistler waves. Under the aspect of the ongoing relaxation by adjustment of the parallel and perpendicular temperature, subsequently wave excitation by the created beam/plateau populations in the absence of temperature anisotropy is considered. In the dispersion analysis, the analytic expressions of the full electromagnetic approach have been used following the formalism described in the textbook [41]. To adapt the desired shapes of the beam/plateau populations, superposition of shifted Maxwellians is taken, similar as done in earlier papers [42] [43] in which plateau distributions played a role.

3.1. Gap Formation by the Downstream Beam/Plateau Population

We start our dispersion analysis with a plasma configuration that is similar to that in former PIC simulations, e.g. in [13] [24] [25]. A two-electron plasma is used with a cold and warm population which are denoted by the subscripts "c" and "w". Their densities and temperatures (given by the plasma beta $\beta_{c,w} = 2\mu_0 n_e k T_{|c,w|} / B_0^2$) are $n_c/n_e = 0.9$, $\beta_c = 2{\cdot}10^{-4}$ and $n_w/n_e = 0.1$, $\beta_w = 0.1$, respectively. n_e is the total electron density. For the warm electron component an anisotropy of $A_w = T_w/T_{\|w} - 1 = 2.0$ was taken by which the whistler waves are driven; the cold electrons are isotropic, *i.e.* $A_c = 0$.

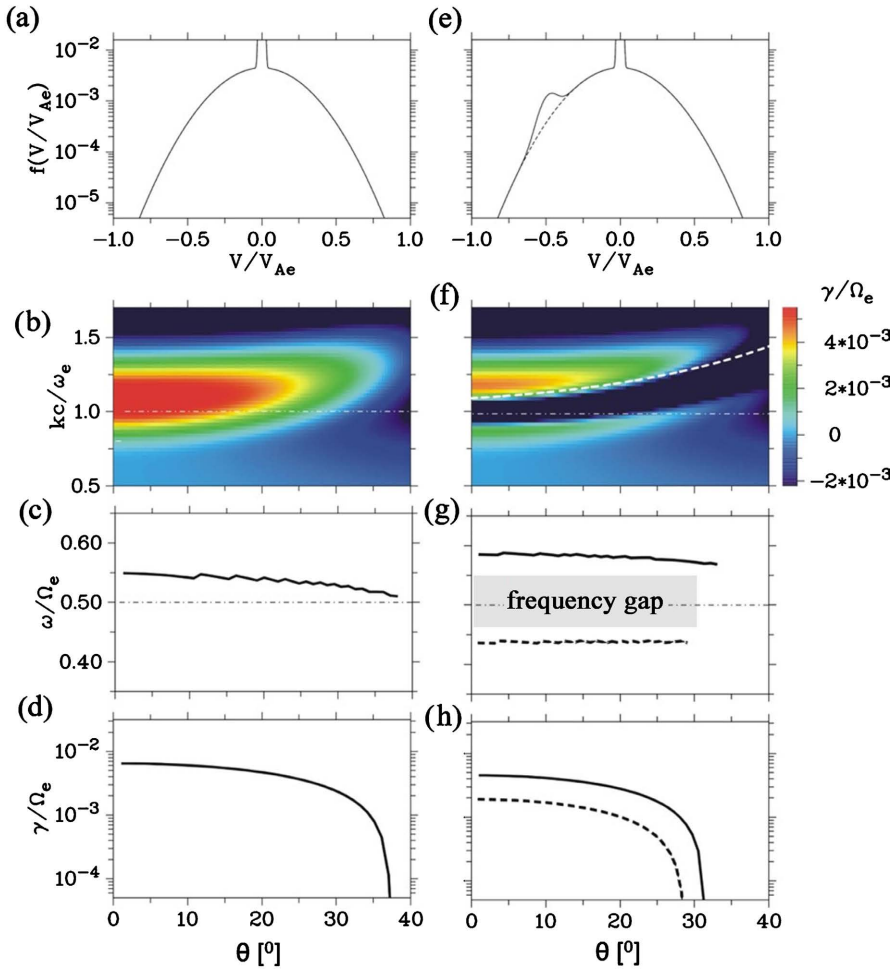

Figure 5. Electron distribution function (parallel to the magnetic field) and related dispersion of whistler waves driven by temperature anisotropy. a) The hot electron population has a density of 10% of the total density ($n_h/n_e = 0.1$) and an electron plasma beta of $\beta_h = 0.1$; a temperature anisotropy of $A_h = 2$ has been taken. In panel (e), a counter-streaming beam/plateau population has been added (parameters: $n_b/n_e = 0.003$, V_b/V_{Ae}~0.47, $T_b/T_w = 0.04$). Panel (b) and (f) show the color-coded growth rate γ/Ω_e versus the propagation angle θ and the wave number kc/ω_e. In panels (c), (g) and (d), (h), the frequency ω/Ω_e at the maximum growth rate and the maximum growth rate itself, respectively, are plotted versus the propagation angle θ. The dotted white line in panel (f) represents the wave number $k(\theta)$ at which the beam-shifted cyclotron mode $\omega = \Omega_e + \boldsymbol{k}\cdot\boldsymbol{V_b}$ ($V_b < 0$) intersects the whistler mode. The dashed lines in panels (g) and (h) belong to the lower maximum of the growth which arises due to the gap formation.

In Figure 5, results of dispersion analysis for two plasma configurations represented by the electron distribution functions in the upper panels (a) and (e) are shown. The difference between the two distributions is that in (e) the Maxwell distribution in (a) has been expanded by a downstream beam/plateau (b/p) population. The parameters of this minor electron component marked by the subscript "b" are: $n_b/n_e = 0.003$, V_b/V_{Ae}~0.47, $T_b/T_w = 0.04$. (The effect caused by an upstream population is considered subsequently.) In both cases, whistler waves are excited by the temperature anisotropy of the warm population. The

color plots of panels (b) and (f) show the growth rate of the whistler instability (γ/Ω_e) versus the wave number kc/ω_e and the propagation angle θ.

Comparing in Figure 5 both color plots, it is evident that the addition of the downstream b/p population generates an area in the k-θ space in which whistler damping instead of wave growth occurs. This 'damping region' is located along the dotted white line in panel f) which represents the θ-variation of the wave number according to Equation (1) at which the b/p cyclotron mode $\omega = \Omega_e + k \cdot V_b$ ($V_b < 0$) intersects the whistler mode, see also Figure 1(c).

The most remarkable effect of the cyclotron resonance damping is the arising frequency gap at $\omega \sim \Omega_e/2$ which is marked in panel (g). This can also be seen in the maximum growth rate in panel (h) which is split into two lines compared to the single maximum (panel (d)) of the pure Maxwellian distribution.

Summarizing the view in Figure 5, one can say that the gap formation at $\omega \sim \Omega_e/2$ is based on the resonance between the cyclotron mode of the downstream b/p population and the whistler mode. To demonstrate this effect from a slightly different perspective, the dispersion characteristics for the electron configurations of Figure 5(a) and Figure 5(e) are shown in Figure 6 for two propagation angles. The electron distribution functions are plotted again in the top panels (a) and (e). In the panels below the growth rate γ/Ω_e is drawn versus the frequency for the propagation angles $\theta = 10^\circ$ (middle panels) and $\theta = 45^\circ$ (bottom panels). The gap formation in panel f) is seen. As mentioned before, it appears at the intersection of the b/p cyclotron mode (dashed-dotted line) with the whistler mode (solid line) of the total electron plasma. In the same way, the cyclotron damping due to the downstream b/p population causes that the weak growth rate of the pure Maxwellian plasma for $\theta = 45^\circ$ (panel (c)) completely disappears in panel (g).

3.2. Wave Generation by Upstream Beam/Plateau Populations

Up to now, modifications of the whistler dispersion properties by a *downstream* b/p population have been considered. As we shall see, the existence of an *upstream* b/p population results in a source of wave excitation due to beam instability. The different roles of the two electron populations are shown schematically in Figure 3. The whistler mode and the two beam modes that are associated with the up- and downstream electrons are plotted there.

Returning to the kinetic dispersion analysis, the completely new situation at the presence of an *upstream* b/p population with regard to the whistler wave excitation is shown in Figure 7. As before, a temperature anisotropy of $A_h = 2$ is assumed. Looking first to the left panels of Figure 7, serious modifications compared with the situation in Figure 5 are evident. The most pronounced signature is the fact that the region of unstable waves is not more restricted to quasi-parallel propagation, but it extends to large propagation angles with a maximum at about 60˚. At the transition from quasi-parallel to oblique propagation, the wave number of maximum growth rate shifts from $kc/\omega_e \sim 1$ to $kc/\omega_e \sim 1.6$ and remains almost constant for $\theta \gtrsim 40^\circ$. The instability in the range of nearly constant

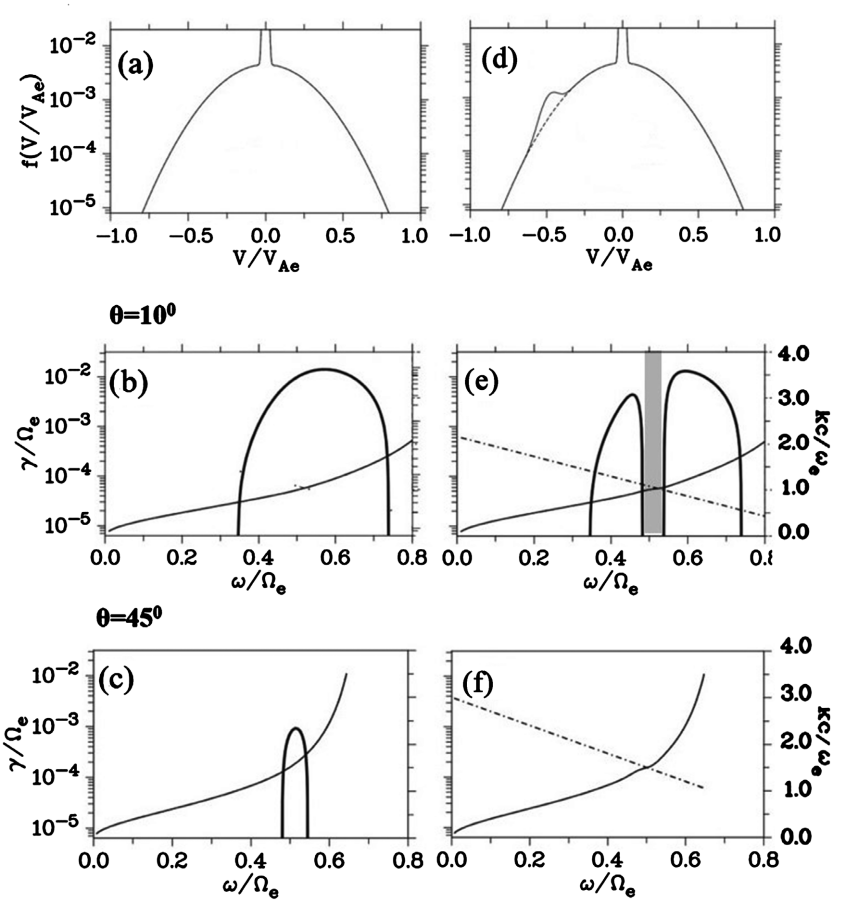

Figure 6. Growth rate versus frequency showing the gap formation by the *downstream* beam/plateau population. For the same distribution functions as in **Figure 5** (top panels), the growth rate is shown for two propagation angles ($\theta = 10^\circ$ and $\theta = 45^\circ$). In panel e), the frequency gap at $\omega \sim \Omega_e/2$ is marked by the grey area. It appears where the beam-shifted cyclotron mode $\omega = \Omega_e - \boldsymbol{k}\cdot\boldsymbol{V_b}$ (dashed-dotted line, $V_b/V_{Ae} = -0.47$) intersects the whistler mode (thin solid line).

wave number ($kc/\omega_e \sim 1.6$) has the character of a beam instability which is caused by the interaction of the beam/plateau mode $\omega \sim \boldsymbol{k}\cdot\boldsymbol{V_b}$ ($V_b > 0$) with the whistler mode. A beam speed of $V_b/V_{Ae} \sim 0.45$ is required to get from Equation (2) the above determined wave number. Accordingly, the frequency plotted as a solid line in **Figure 7(c)** varies with the propagation angle θ (for $\theta > 30^\circ$) as $\omega \sim 0.75\cdot\cos\theta$.

Another remarkable feature is the appearance of the lower-frequency beam mode, seen in color plot of **Figure 7(b)**) as a blue strip at $kc/\omega_e \sim 0.5$ and plotted in panels (c) and (d) as dotted lines. In agreement with the prediction of Equations (3) and (4), its frequency varies with θ as $\omega \sim 0.25\cdot\cos\theta$. This mode reaches its maximum at $\theta \sim 60^\circ$ with a growth rate which is about one order less than that of the "upper beam instability" with $kc/\omega_e \sim 1.6$. In the right panels of **Figure 7** the damping effect of the cyclotron mode—as described before—becomes evident for the case that the *downstream* beam/plateau population is added. As seen in **Figure 7(f)**, the "absorption region" in the $k - \theta$ space is again located

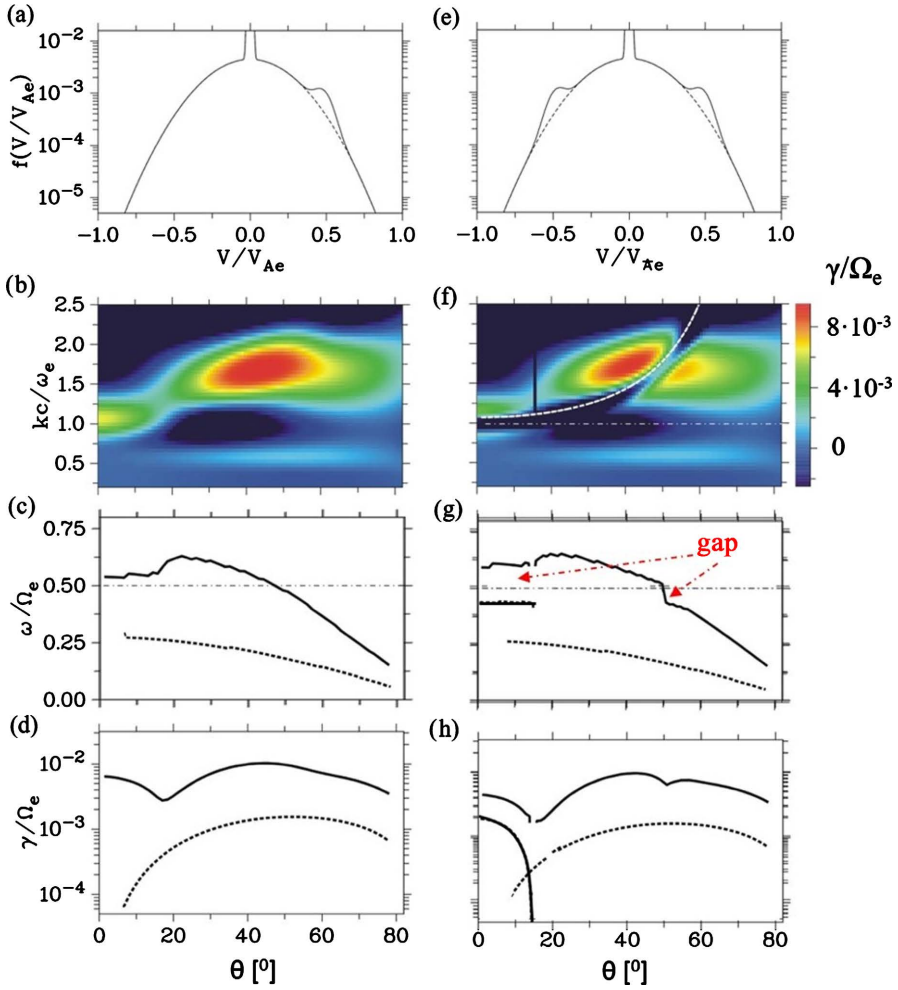

Figure 7. Whistler wave generation by temperature anisotropy (A_h = 2). Otherwise, the format is the same as in **Figure 5**. An important new feature, however, is the presence of an *upstream* beam/plateau population in the distribution function of panel (a). In (e), both populations, up-and downstream, are present. Note the appearance of a second frequency gap near $\omega = \Omega_e/2$ (kc/Ω_e~2) at oblique propagation (θ~50˚) and the appearance of the lower-frequency beam instability at kc/ω_e~0.5 in the color plots of panels (b) and (f). Its frequency and growth rate are shown in panels (c), (g) and (d), (h), respectively, as dotted lines.

along the dotted white line which represents the k versus θ variation of the intersection point between the cyclotron mode $\omega = \Omega_e + \boldsymbol{k}\cdot\boldsymbol{V_b}$ (V_b~−0.5 V_{Ae}) and the whistler mode. As in **Figure 6(e)**, in the range of quasi-parallel waves the frequency gap at ω~$\Omega_e/2$ (kc/Ω_e~2) is formed. Additionally, a second frequency gap may arise for obliquely propagating waves at $\theta \gtrsim 50^\circ$. It is caused by the simultaneous interaction of the two beam/plateau modes with the whistler mode, as sketched in **Figure 3(b)**. Otherwise, the signatures are similar as in the left panels: 1) constant wave number in the range of beam-generated waves, 2) frequency variation with cosθ, 3) occurrence of the lower-frequency beam instability.

To better illustrate how the growth rate is dependent on the frequency, **Figure 8** shows the growth rate for three propagation angles, $\theta = 10^\circ$, 45˚, and 60˚. The

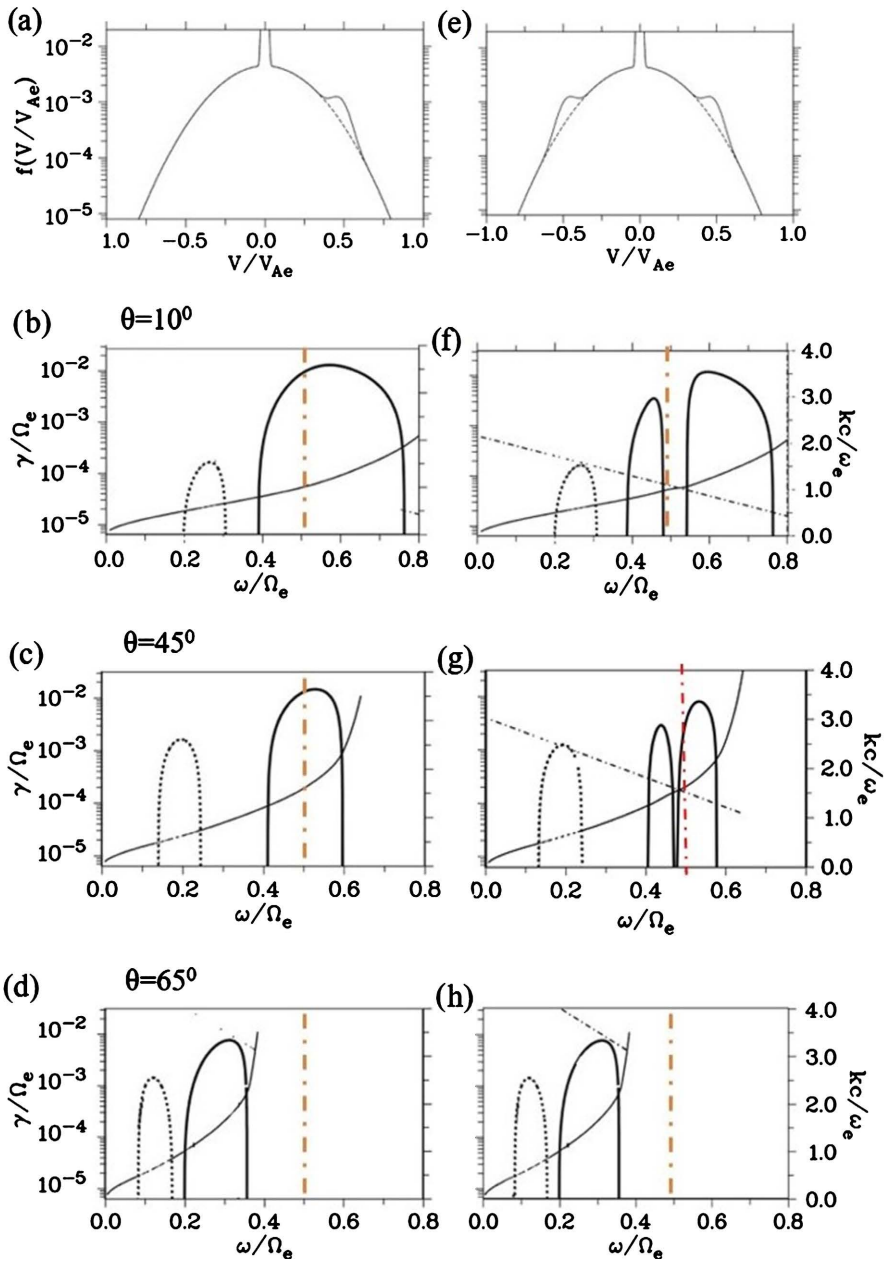

Figure 8. For the conditions of **Figure 5**, the growth rate versus frequency is shown for three propagation angles (θ = 10˚, 45˚ and 65˚). Otherwise, the format is the same as in **Figure 6**. As there, a frequency gap at $\omega \sim \Omega_e/2$ is formed by quasi-parallel waves (panel (f)). Note that in **Figure 8(g)** another gap around the same frequency for obliquely propagating waves (θ~45˚) exists. It is obviously related to the presence of both b/p populations. For θ = 65˚, the *downstream* b/p population has no effect more on the beam instability. The dotted curves in panels (b)-(h) indicate the lower-frequency instability at the crossing point of beam and whistler mode.

gap formation seen in **Figure 8(f)** is a common feature for quasi-parallel whistler waves driven by the temperature anisotropy at the presence of a down-stream b/p population of resonant electrons.

The second frequency gap at θ~45˚ (**Figure 8(g)**), on the other hand, is based

on the simultaneous existence of the two beam/plateau populations, the upstream population causing wave excitation and the downstream population, which ensures the frequency-selective damping. This mechanism can unambiguously identified by comparing the rate of growth γ/Ω_e versus frequency ω/Ω_e in the right and left panels. The dotted curves in the panels (b)-(d) and (f)-(h) around $\omega \lesssim 0.2\Omega_e$ belong to the (lower-) beam instability which arises at the low-frequency cutting point of the b/p mode $\omega \sim \boldsymbol{k} \cdot \boldsymbol{V}_b$ with the whistler mode.

Although its maximum amplitude is about one order of magnitude below that of the upper beam instability, it seems to be relevant for space observations, as we discuss later.

To underline the great relevance of the b/p populations, in Figure 9 results of

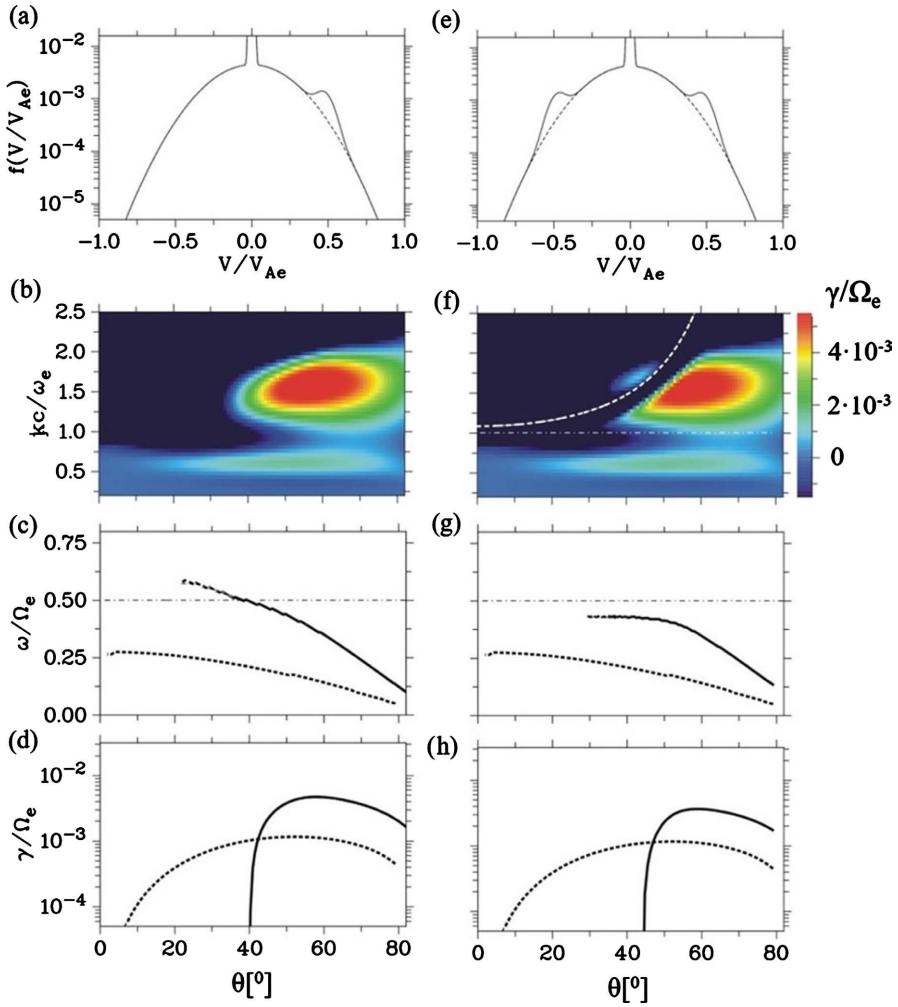

Figure 9. Whistler wave generation (without temperature anisotropy) by a *upstream* beam/plateau population (panel (a)) and onset of damping if simultaneously *downstream* electrons are present (panel (b)). The wave activity reaches its maximum at about 60˚ at low-band frequencies of $\omega/\Omega_e \sim 0.4$. In this range of propagation angles θ another lower-frequency whistler wave of smaller amplitude exist with $kc/\omega_e \sim 0.5$ and $\omega/\Omega_e \sim 0.2$, seen as a light blue strip in panels (b) and (f) and as dotted curves in the panels (c), (d) and (g), (h). The dotted white "absorption" line in the color plot of panel (f) has been explained in Section 2.1.

the dispersion analysis are shown for the case that—in comparison to the situation in Figure 7—the resonant energetic electrons are the only source of whistler waves. Such a situation can be imagined after the original instability due to the temperature anisotropy has relaxed and the associated waves are damped away. The lack of temperature anisotropy instability in Figure 9(b) and Figure 9(f) is indicated by the absence of whistler wave activity with kc/ω_e~1 in the range of quasi-parallel propagation ($\theta \lesssim 30^\circ$). The growth rate for obliquely propagating waves generated by the b/p instability, on the other hand, is only weakly influenced in comparison with the situation in Figure 7. The frequency follows the expression (2) and is located between the Gendrin and the resonance cone angle. The maximum growth rate occurs at about 60˚. By the reduced growth rate in the range around $\theta \lesssim 50^\circ$ compared with the values in Figure 7, there are no upper-band waves and the frequency gap of obliquely propagating waves, seen in Figure 7(f), almost disappears. Indeed, the lower-frequency b/p instability ($\omega \lesssim 0.2\Omega_e$) is nearly unaffected by the absence of the temperature anisotropy.

Finally, slightly different distribution functions of resonant electrons have been used in order to investigate their influence on the b/p instability. In Figure 10(a), two b/p distributions with V_b~$0.5\,V_{Ae}$ are shown which have the same density (n_b/n_e = 0.005), but differ slightly in shape by shifting the left border of the beam/plateau (generated by superposition of Maxwellians) a little to smaller values. In this way, a transition from a beam ($\mathrm{d}f/\mathrm{d}v \gtrsim 0$, solid curve) to a real plateau (dashed curve) with $\mathrm{d}f/\mathrm{d}v \lesssim 0$ has been realized. As expected, that has no effect on the ω (real)-θ variation shown in Figure 10(b). However, a significant change in the growth rate (Figure 10(c)) is obvious. At transition to a plateau a shift of the wave activity to larger propagation angles, associated with an amplitude reduction, takes place. As a remarkable feature one has to note that for a strict plateau with $\mathrm{d}f/\mathrm{d}V \lesssim 0$ a weak instability (dashed curve in Figure 10(c)) is still retained. Which distribution function of resonance electrons exists can only be obtained from kinetic simulations, ultimately 2D, which take into account all relevant plasma parameters such as electron plasma beta and temperature anisotropy.

4. Three Further Cases: β_e = 0.01, β_h = 0.2 and β_h = 0.4

In the previous section we discussed the consequences of resonant b/p populations on whistler wave generation for the special case of β_w = 0.1. It was selected with the emphasis on the gap formation of quasi-parallel waves in an anisotropic plasma. In order to allow more general conclusions regarding the interpretation of magnetospheric whistler wave observations, comparable results of the dispersion analysis are shown in Figure 11 for three plasma betas covering the characteristic features of unstable cold (β_c = 0.01) and warm plasmas (β_w = 0.2, 0.4).

The left panels of Figure 11 show the results of dispersion analysis for β_c = 0.01. That is a case for which in the pure Maxwellian plasma because of the plasma beta below the critical value (β_{cr} = 0.025), only waves at ω~$0.65\Omega_e$ by a

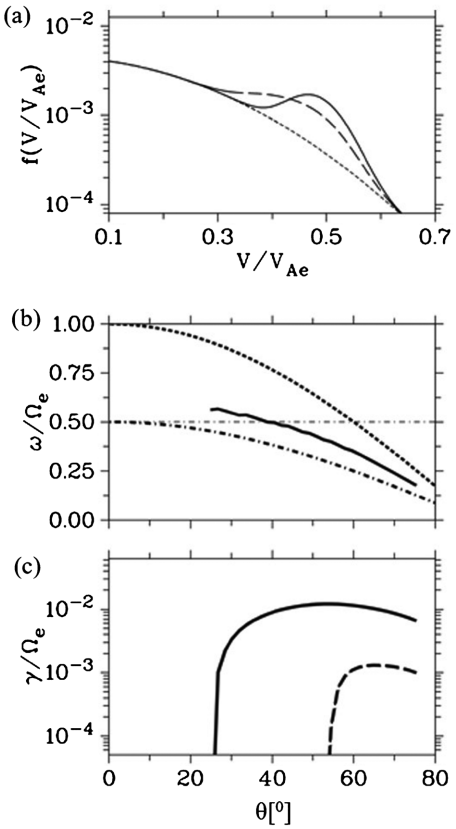

Figure 10. Influence of the velocity distribution of the beam/plateau electrons on the whistler wave instability. The beam/plateau density is $n_b/n_e = 0.005$ (instead of 0.003 as used in **Figure 6**). (a) The shape of the distribution function at $V_b/V_{Ae} \lesssim 0.5$ has been changed by shifting the lower border of the velocity range of superposed Maxwellians from 0.45 (solid line) to 0.36 (dashed line). The wave frequency ω/Ω_e and the growth rate γ/Ω_e versus the propagation angle θ are shown in panels (b) and (c), respectively. The dashed-dotted and dotted curves in panel b) represent the Gendrin and resonance cone angle, respectively.

temperature anisotropy are excited. Their maximum growth rate is at $\theta \sim 50^\circ$, see e.g. [9] [10] and [23]. As seen in **Figure 9(b)** and **Figure 9(c)**, the same also happens if the distribution function in (a) is modified by resonant b/p populations. Different, however, is the extension of comparable wave activity to higher propagation angles and the existence of a clear gap at $\omega \sim \Omega_e/2$ ($kc/\Omega_e \sim 4$) in that range. This feature is retained even in the case that there is no temperature anisotropy, as seen in the lower panels (d) and (e). In this way, the whistler wave activity may extend with increasing propagation angle from the upper band ($\omega \gtrsim \Omega_e/2$) to the lower band ($\omega \lesssim \Omega_e/2$) with a gap in between. The maximum growth rate is at about $\theta = 65^\circ$.

The results shown in the middle and right panels for $\beta_w = 0.2$ and $\beta_w = 0.4$, respectively, are not so much different from those described in Section 3 for $\beta_w = 0.1$. On both cases one has it to do with super-critical electron plasma ($\beta_e > 0.025$) for which the maximum growth rate of temperature anisotropy instability is at parallel propagation. Notable results concern the required conditions of gap

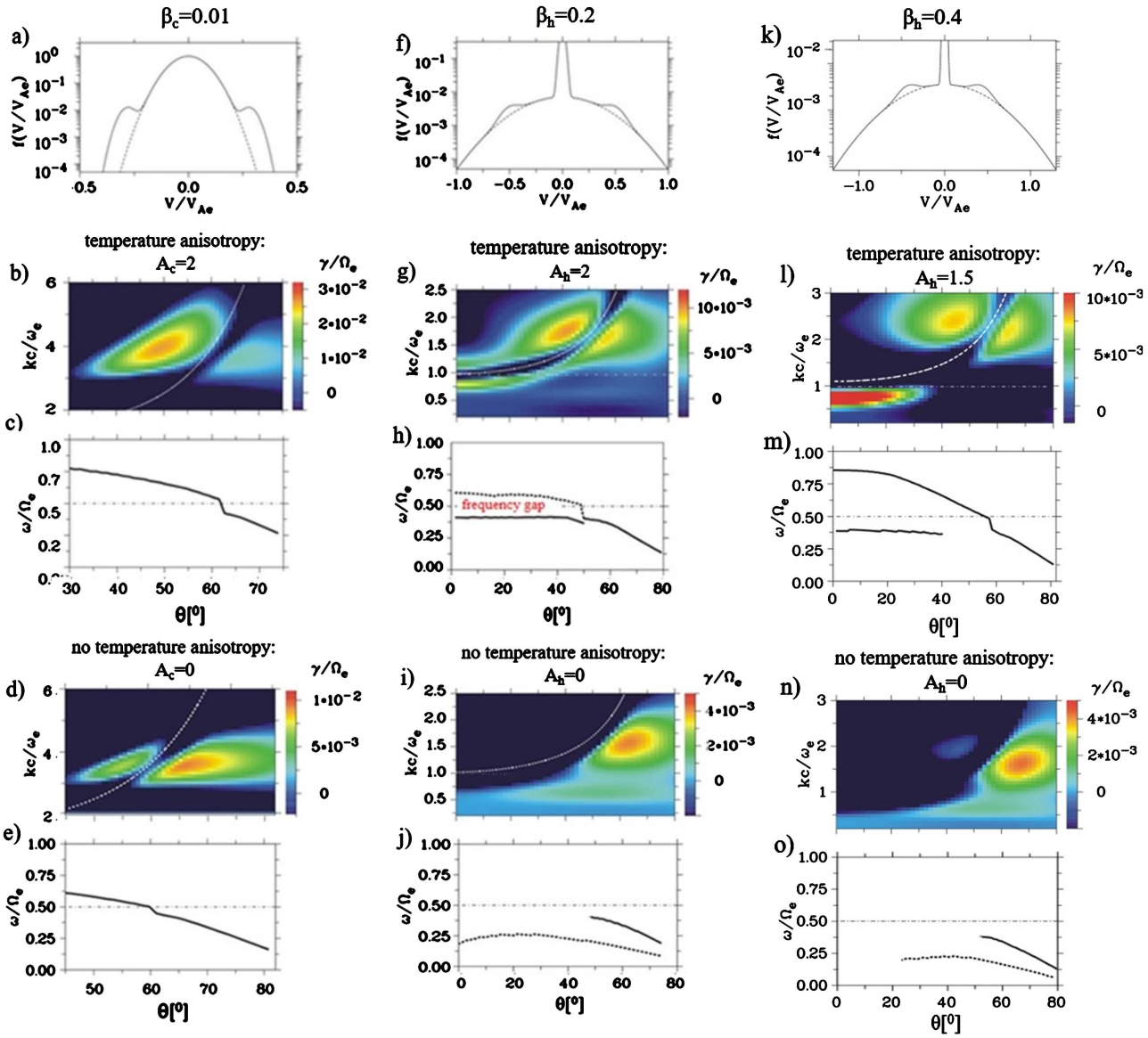

Figure 11. Whistler wave generation in the presence of up- and downstream beam/plateau populations with and without temperature anisotropy. Panels (a)-(e) are for a cold (single) electron plasma with $\beta_c = 0.01$ and b/p parameters of $n_b/n_e = 0.005$, $V_b/V_{Ae} = 0.3$; panels (f)-(j) and (k)-(o) belong to warm two-electron plasmas ($n_w/n_e = 0.1$) with $\beta_w = 0.2$ and $\beta_w = 0.4$, respectively. The b/p parameters are $n_b/n_e = 0.005$ and $V_b/V_{Ae} = 0.5$. The dotted curves in panel j) and o) represent the lower-beam instability. Whether a temperature anisotropy is present or not is indicated in the figure.

formation with regard to β_w. Different situations are seen in the color panels g) and l) showing the growth rate versus ω and θ. While for $\beta_w = 0.2$ the symmetrical growth rate around $kc/\omega_e = 1$ leads to a well-defined frequency gap that extends up to θ~50˚ (also marked in Figure 11(h)), no gap formation due to quasi-parallel waves is possible if β_w increases to 0.4, which shifts the wavenumber of maximum growth to a smaller value. Further, a remarkable result is a fact that for all three cases in which the wave excitation is based exclusively on the existence of the b/p populations (lower two panels in Figure 11), the maximum growth rate occurs at θ ~60˚.

5. Discussion

Based on the results of Section 2 and the supplementary analysis in Section 3, some of the most important phenomena of magnetospheric whistler waves are discussed with regard to their origin.

5.1. Gap Formation at $\omega \sim \Omega_e/2$

The first point of our discussion concerns the gap formation. Depending on the source of the whistler waves involved, two types of frequency gaps are to be distinguished; one for quasi-parallel waves driven by temperature anisotropy and the other for oblique waves which are generated by the *upstream* beam/plateau population. In both cases, the gaps are caused by the cyclotron damping of the b/p mode $\omega \sim \Omega_e + \boldsymbol{k} \cdot \boldsymbol{V_b}$ ($V_b < 0$) which belongs to the resonant *downstream* electrons ($V_b < 0$) and crosses the whistler mode at $\omega \sim \Omega_e/2$.

Gaps of quasi-parallel waves which are based on self-consistent deformations of the electron distribution function have been studied in recent papers, beginning with the 2D PIC simulations of [13]. They have shown that selective reduction of the whistler wave growth rate is caused by a deformation of the electron distribution function at that point in the velocity space where the resonant interaction between the unstable wave and the electrons takes place and a plateau is formed. In the paper [14], gap formation, seen in 1D PIC simulations, has been interpreted by splitting the anisotropic electrons into two energy ranges, which are separated by a more isotropic one as a consequence of parallel resonant Landau acceleration. The physical relevance of the beam/plateau related cyclotron mode is first considered in the paper of [10] in which, furthermore, the excitation of oblique whistler waves and related gap formation (at the absence of temperature anisotropy) by the combined action of resonant up- and downstream electrons have been analysed. It should be noted, however, that the cyclotron damping of the whistler waves near $\Omega_e/2$ by the added b/p population is equivalent to a local suppression of the initial temperature anisotropy at cyclotron resonance, in agreement with the results of the numerical simulations in [13] [14].

In paper [32] the characteristics of whistler waves excited by temperature anisotropic electrons whose distribution function is a combination of a bi-Maxwellian and minor beam/plateau-like modifications have been investigated by both linear theory and PIC simulations. Special emphasis was directed on the influence of the beam/plateau parameters (density, velocity) on the gap position. In the subsequent papers [24] [25] parts of these predictions have been checked by 1D/2D PIC simulations. For fixed propagation angle of $\theta = 20^\circ$, the authors confirmed our above conclusions after which a frequency gap of quasi-parallel propagating waves can only be formed in warm plasmas in the range $0.05 \lesssim \beta_w \lesssim 0.2$.

The outcome of our analysis of two types of gaps seems to be very important with regard to interpretation of the magnetospheric gap observations. In [4]

have been classified gap events and found out one class which have in common that the gap occurs when θ rises above the Gendrin angle θ_G or even starts to spread out over a broad range of angles (up to 55˚) the closer it gets to $\Omega_e/2$. Similarly, published spectra in which the frequency gap at $\Omega_e/2$ occurs around $\theta =$ 60˚, close to the resonance cone angle [44]. Furthermore, the statistical analysis in [7] revealed that banded emission exists in a broad range of propagation angles reaching from the Gendrin angle [45] up to the resonance cone. These results fully confirm our conclusions about the essential role of the resonant b/p populations for both wave generation and gap formation.

Finally, it should be mentioned that whistler wave emission over a broad frequency range without a gap has been observed in e.g. [4] [7] and [46]. Looking at the ω-θ distribution of the no-gap and banded whistler waves in **Figure 4** in [7], one gets the impression that both kinds of waves have the same origin. The simplest reason for the partially observed lack of gaps seems to be a missing downstream b/p population that rules out frequency-selective cyclotron damping as the causative mechanism. Hereby, asymmetries by plasma drift and spatial inhomogeneities may play a role. Further, it is noteworthy that most chorus wave observations mentioned above that exceeded $0.5\Omega_e$ exhibits a weak low-frequency line with a nearly constant frequency of ω~$0.2\Omega_e$. Since the corresponding wave normal angle is not given there, unfortunately, it remains unclear whether a beam/plateau population is the possible origin of this weak wave activity.

5.2. Generation of Lower-Band Oblique Waves

Another challenging point with respect to our theoretical studies is the debate about the wave normal angle distribution of the waves in the lower band. In addition to the peak within about 20˚, a second peak was observed at oblique angles near the resonance cone, e.g. in [28] [47] [48] and in [7]. While the quasi-parallel waves can be related to temperature anisotropy, the source of the oblique waves of the lower band remained largely open. In this context, we refer to the simple relationships (3) and (4), according to which the frequency of the b/p generated waves versus the propagation angle is given by $\omega = 0.5\Omega_e A\cos\theta$, where A varies between $A = 1$ (Gendrin angle) and $A = 2$ (resonance cone). Besides, our dispersion analysis whose main results are reviewed in **Figure 11** shows that the growth rate of beam-generated whistler waves (ignoring temperature anisotropy) is located at θ~60˚. Thus, assuming A~1.5 as a middle between Gendrin and resonance cone angle, the associated frequency would be ω~$0.38\Omega_e$. Such a type of waves based on simultaneous observations of low-energy electron streams (beams and/or plateaus) have been discussed in the literature, e.g., in [14] [28] [49] [50] [51] and in [29]. It has been found in [28] that measured electron distribution functions having a plateau/beam-like shape are directly correlated with a positive growth rate of whistler waves at very oblique propagation ($\theta \gtrsim 60$˚). Additionally, weaker whistler activity at $\omega < 0.2\Omega_e$ is mentioned there which in

our view may arise owing to the lower-beam instability, see e.g. **Figure 9(j)** and **Figure 9(o)**.

An obvious relation between lower-band chorus waves and beam-like distributions has been described in [29]. As a clear signature, the measured plateau at a velocity of $V_b \sim V_{Ae}/2$ is correlated with whistler waves at $\omega/\Omega_e \sim 0.23$ propagating close to $\theta = 70^\circ$ (denoted there as Event II waves). Also there, a wave at a lower frequency ($\omega/\Omega_e \sim 0.13$)—not further discussed there—is simultaneously observed which again seems to us is another indicator of the presence of a beam that is responsible for both lower-band emissions. For an understanding of the process by which the electron distribution with a beam/plateau is generated, one has to mention that quasi-parallel whistler waves in the lower band also exist (Event I waves). To drive the Event I waves unstable by reasonable temperature anisotropy, according to the dispersion analysis (see **Figure 11(m)**), an electron plasma beta of $\beta_w \gtrsim 0.4$ is required.

The described in [29] observation is directly related to the earlier conclusions in [31], where it was explained the statistically found rarity of simultaneous observations of intense parallel and oblique waves in the lower band by means of beam/plateau formation. The following mechanism is suggested: Initial temperature anisotropy generates quasi-parallel whistler waves associated with a modified distribution function owing to resonant electrons. Subsequently, very oblique waves ($\theta \gtrsim 60^\circ$) are amplified, whereas the parallel waves are supressed by increasing damping.

Further the existence of the beam/plateau modes $\omega = \boldsymbol{k} \cdot \boldsymbol{V_b}$ seems to be an important aspect in the formation of the so-called QE-MBC (quasi-electrostatic multiband) events, as described in [5]. In the case of the primary excited lower-band chorus with propagation angles of about 70˚, the observation of the second and third harmonic (see their **Figure 2**) suggests beam excitation, whereby the energy (ω) and impulse (k) conditions for three-wave interaction are immediately fulfilled, similar as for the harmonics of the electron plasma frequency at beam-plasma interaction [20]. Similarly, beam modes seem to be involved in the analogous EM (electromagnetic)-MBC events which occur at quasi-parallel propagation.

Finally, it would be worth adding that in the present work we have exclusively assumed that the beam/plateau is formed by resonant electrons of the initially unstable whistler waves. However, plateau formation can also occur through other types of waves, such as kinetic Alfvén waves, time domain structures or ion outflow, even before a whistler-mode wave was excited [30].

5.3. Few Remarks to the Chirping

With the theoretical evidence that whistler waves can be generated by resonant beam/plateau populations, the question arises to what extent this mechanism is involved in the formation of chorus waves which occur in form of rising and falling tones, e.g. in [2] [52] [53] [54]. A comprehensive classification of differ-

ent chorus events has been done in [4] who distinguished five groups among the most common rising tones: group 1: crossing $0.5\Omega_e$ with $\theta < \theta_G$ (Gendrin angle) in lower band, group 2: frequency gap in emission at $0.5\Omega_e$, group 3: crossing $0.5\Omega_e$ with $\theta_G < \theta < \theta_r$ (resonance cone), group 4: the lower band only ($<0.5\Omega_e$), and group 5: the upper band only ($>0.5\Omega_e$).

The events of group 1 and group 2 in [4] belong to the quasi-parallel waves ($\theta < 30^\circ$), and they are related to our studies in Section 3.1 after which unstable waves covering $0.5\Omega_e$ are generated by temperature anisotropy, provided the plasma beta of the hot electron component (β_h) is in the range $0.05 \lesssim \beta_h \lesssim 0.3$. As further shown in **Figure 5** and **Figure 6**, to form a gap the presence of a downstream beam/plasma population with velocities $V_b \sim 0.5\, V_{Ae}$ is required. Our view that the waves of group 1 and 2 have the same origin is supported by the following observation in [4]: For both groups almost identical traces in the θ-ω plane of the scanned bursts outside the gap area have been obtained; see **Figure 4(a)** and **Figure 4(b)** therein.

All chorus bursts of group 2 have in common that the frequency gap occurs when θ rises above the Gendrin angle θ_G. For some events, θ starts to spread up to about 55˚ if it gets close towards the gap. In our view, this behavior indicates the presence of hot electron plasma ($\beta_h \gtrsim 0.3$) whose maximum growth rate owing to temperature anisotropy is shifted below $\Omega_e/2$ and thus a frequency gap can only be formed by resonant b/p populations at oblique wave propagation. Such a situation has been shown in **Figures 11(k)-(m)**. In **Figure 12**, as modification of **Figure 8(m)** the propagation angle θ versus the frequency ω/Ω_e is plotted, including the Gendrin and resonance cone angle θ_G and θ_{rc}, respectively. As seen, it has much similarity with **Figure 3(c)** in [4]. The strongest emission is outside the Gendrin angle θ_G in the range of quasi-parallel propagation ($\theta \lesssim 30^\circ$) and with a frequency of $\omega \sim 0.4\Omega_e$. The wave activity between θ_G and θ_{rc} which is caused by the (upstream) b/p population stretches from about $\omega/\Omega_e = 0.25$ to about 0.7 whereby the angle θ drops from about 70˚ down to about 30˚.

The group 3 events of [4] can be classified in a similar way. These exhibit no pronounced gap and are characterized by constantly raising frequency as the angle

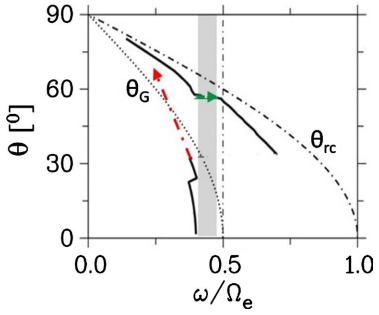

Figure 12. Modified version of **Figure 11(m)** showing the propagation angle θ versus the frequency ω/Ω_e from dispersion analysis (solid lines). The plasma beta of the hot electron component is $\beta_h = 0.4$. The dotted and dashed-dotted curves represent the Gendrin (θ_G) and resonance cone angle (θ_{rc}), respectively.

θ decreases, with $\theta_G < \theta < \theta_{rc}$ always applying. That means, the picture is similar as in **Figure 9**, however, without wave activity below the Gendrin angle θ_G. This brings us back to Section 3.2 in which whistler wave generation by upstream beam/plateau populations has been analysed. The main characteristic of these waves is their ω-θ variation which according to Equation (2) follows as $\omega = 0.5\Omega_e A\cos\theta$ where A varies between $A = 1$ (Gendrin angle) and $A = 2$ (resonance cone) depending on the beam/plateau velocity, see Equation (3). Further, in the representations of riser elements investigated in [55], especially in their Figure A1, there is a striking observation that seems to be closely related to our investigations. In addition to the measurements of lower-band risers of quasi-parallel waves, subsequent chorus events in distances of about one second that spread over angles between 60˚ and 90˚ are seen as a signature of beam-driven waves.

One point that has not been considered so far concerns the fine structure of the chorus events. It has already been analyzed in the past (e.g. [53] [56] [57] [58] and has recently received new impetus from research in [55] and [59] [60] on lower-band chorus risers, which present themselves as a series of monochromatic wave packets.

Due to the fact that for sufficiently hot electron plasmas ($\beta_e > 0.025$) the phase velocity of the unstable whistler waves is very close to $0.5\,VA_e$, the inflection point where phase and group velocity coincide and have a maximum, the interpretation comes to mind that these "coherent" waves are connected to whistler oscillitons, a type of solitons ([61] [62]). This class of solitons arises due to the periodic momentum exchange between the electrons and protons, mediated by Maxwell stresses, giving rise to wave packet structures. Wave packets for classical whistler waves appear due to nonlinear beating between wave motions of the electrons and protons due to a small difference of their phases. In plasma with electron beams a beating can occur between wave motions of the bulk and beam electrons. The feature of the inflection point with maximum of the group velocity on the dispersion curve is that wave packets will be gathered there. The phase mixing of waves in the vicinity of the inflection point with maximum of the phase speed is very small. This concept has been applied to the interpretation of STEREO radiation belt and auroral hiss observations ([19] [40]).

Besides the observations in [55], who showed that some short wave packets seem to have nearly constant frequency, it means they are nearly monochromatic with $\mathrm{d}f/\mathrm{d}t \sim 0$, the statistic of short chorus wave packets in [59] [60] more often show a significant variation of the wave frequency over their duration. Such short wave packets have been interpreted, in agreement with nonlinear chorus wave simulations [63], as result of a superposition of two waves whose frequencies are separated by $\Delta\omega/\Omega_e \sim 0.06$. In fact, more recent studies using realistic simulations of non-linear chorus wave generation have shown that two superposed intense waves are often simultaneously generated with a minimum frequency difference imposed by the criterion for resonance non-overlap [64] in good agreement with satellite observations, explaining the formation of short

chorus packets [65] [66].

6. Conclusions

Altogether, our investigations have shown that the interpretation of the spectral properties of magnetospheric chorus waves, originally driven by temperature anisotropy, makes it necessary to include the influence of the self-generated modifications of the electron distribution function owing to resonant electrons into the considerations. In our approach, these are taken into account in the form of beam/plateau (b/p) populations in the kinetic dispersion theory and analysed for their consequences with regard to additional instabilities and damping. Three essential points should be underlined: 1) Cyclotron damping by the downstream b/p population creates the frequency gap at $\Omega_e/2$ for quasi-parallel waves driven by temperature anisotropy. 2) The beam instability associated with the upstream population is the source of whistler waves oblique propagation in the angular range between the Gendrin and the resonance cone angle. 3) The intersection of both beam modes at $\omega = \Omega_e/2$—independently of the beam velocity—and their simultaneous interaction with the whistler wave of defined propagation direction makes the gap formation at half the electron cyclotron frequency to a unique phenomenon of magnetospheric whistler wave generation. In a separate work, 1D particle (PIC) simulations are in preparation to check different aspects of the presented linear theory.

At the end of the Conclusion, we would like to point out that the present work has only considered the linear aspects of wave generation assuming a deformed electron distribution function. However, both parallel and oblique rising and falling tone chorus waves are formed during nonlinear wave generation ([11] [49] [50] [63] [65] [67]). Nonlinear processes, which can lead to beam/plateau formation ([13] [14] [24] [25] [27] [31]) have to be considered in the future together with linear wave excitation to provide a full picture of whistler-mode wave generation.

Acknowledgements

The work was supported by the Strategic Priority Research Program of Chinese Academy of Sciences, Grant No. XDB 41000000. The paper is theoretical and does not use external data.

Conflicts of Interest

The authors declare no conflicts of interest regarding the publication of this paper.

References

[1] Tsurutani, B.T. and Smith, E.J. (1974) *Journal of Geophysical Research*, **79**, 118-127. https://doi.org/10.1029/JA079i001p00118

[2] Burtis, W.J. and Helliwell, R.A. (1969 *Journal of Geophysical Research*, **74**,

3002-3010. https://doi.org/10.1029/JA074i011p03002

[3] Santolik, O., Gurnett, D.A., Pickett, J.S., Grimald, S., Décreau, P.M.E., Parrot, M., *et al.* (2010) *Journal of Geophysical Research*: *Space Physics*, **115**, Article ID: A00F16. https://doi.org/10.1029/2009JA015218

[4] Taubenschuss, U., Santolík, O., Graham, D.B., Fu, H., Khotyaintsev, Y.V. and Le Contel, O. (2015) *Geophysical Research Letters*, **42**, 8271-8279. https://doi.org/10.1002/2015GL066004

[5] Gao, X., Lu, Q. and Wang, S. (2018) *Journal of Geophysical Research*: *Space Physics*, **123**, 5506-5515. https://doi.org/10.1029/2018JA025393

[6] Gao, X., Chen, L., Li, W., Lu, Q. and Wang, S. (2019) *Geophysical Research Letters*, **46**, 4098-4105. https://doi.org/10.1029/2019GL082140

[7] Teng, S., Tao, X. and Li, W. (2019) *Geophysical Research Letters*, **46**, 3607-3614. https://doi.org/10.1029/2019GL082161

[8] Liu, K.J., Gary, S.P. and Winske, D. (2011) *Geophysical Research Letters*, **38**, Article ID: L14108. https://doi.org/10.1029/2011GL048375

[9] Fu, X.R., Cowee, M.M., Friedel, R.H., Funsten, H.O., Gary, S.P., Hospodarsky, G.B., Kletzing, C., Kurth, W., Larsen, B.A., *et al.* (2014) *Journal of Geophysical Research*: *Space Physics*, **119**, 8288-8298. https://doi.org/10.1002/2014JA020364

[10] Sauer, K., Baumgärtel, K. and Sydora, R. (2020) *Earth and Planetary Physics*, **4**, 138-150. https://doi.org/10.26464/epp2020020

[11] Omura, Y., Katoh, Y. and Summers, D. (2008) *Journal of Geophysical Research*: *Space Physics*, **113**, Article ID: A04223. https://doi.org/10.1029/2007JA012622

[12] Omura, Y., Hikishima, M., Katoh, Y., Summers, D. and Yagitani, S. (2009) *Journal of Geophysical Research*: *Space Physics*, **114**, Article ID: A07217. https://doi.org/10.1029/2009JA014206

[13] Ratcliffe, H. and Watt, C.E.J. (2017) *Journal of Geophysical Research*: *Space Physics*, **122**, 8166-8180. https://doi.org/10.1002/2017JA024399

[14] Li, J.X., Bortnik, J., An, X., Li, W., Angelopoulos, V., Thorne, R.M., Russell, C.T., *et al.* (2019) *Nature Communications*, **10**, Article No. 4672. https://doi.org/10.1038/s41467-019-12561-3

[15] Thompson, P., Dougherty, M.K. and Southwood, D.J. (1995) *Planetary and Space Science*, **43**, 625-634. https://doi.org/10.1016/0032-0633(94)00197-Y

[16] Sauer, K., Dubinin, E. and McKenzie, J.F. (2001) *Geophysical Research Letters*, **28**, 3589-3592. https://doi.org/10.1029/2001GL013047

[17] Moullard, O., Burgess, D., Salem, C., Mangeney, A., Larson, D.E. and Bale, S.D. (2001) *Journal of Geophysical Research*: *Space Physics*, **106**, 8301-8313. https://doi.org/10.1029/2000JA900144

[18] Graham, D.B. and Cairns, I.H. (2013) *Journal of Geophysical Research*: *Space Physics*, **119**, 2430-2457. https://doi.org/10.1002/2013JA019425

[19] Sauer, K. and Sydora, R.D. (2011) *Annals of Geophysics*, **29**, 1739-1753. https://doi.org/10.5194/angeo-29-1739-2011

[20] Sauer, K. and Sydora, R.D. (2012) *Plasma Physics and Controlled Fusion*, **54**, Article ID: 124045. https://doi.org/10.1088/0741-3335/54/12/124045

[21] Sauer, K., Baumgärtel, K. and Sydora, R. (2020) *Earth and Planetary Physics*, **4**, 1-13. https://doi.org/10.26464/epp2020020

[22] Schriver, D., Ashour-Abdalla, M., Coroniti, F.V., LeBoeuf, J.N., Decyk, V., Travnicek, P., Santolík, O., Winningham, D., Pickett, J.S., *et al.* (2010) *Journal of Geo-*

physical Research: *Space Physics*, **115**, Article ID: A00F17. https://doi.org/10.1029/2009JA014932

[23] Gary, S.P., Liu, K, J. and Winske, D. (2011) *Physics of Plasmas*, **18**, Article ID: 082902. https://doi.org/10.1063/1.3610378

[24] Chen, H., Gao, X., Lu, Q., Sauer, K., Chen, R., Yao, J. and Wang, S. (2021) *Journal of Geophysical Research*: *Space Physics*, **126**, e2020JA028631. https://doi.org/10.1029/2020JA028631

[25] Chen, H., Gao, X., Lu, Q., Fan, K., Ke, Y.,Wang, X. and Wang, S. (2022) *Journal of Geophysical Research*: *Space Physics*, **127**, e2021JA030119. https://doi.org/10.1029/2021JA030119

[26] Min, K., Liu, K.J. and Li, W. (2014) *Journal of Geophysical Research*: *Space Physics*, **119**, 5551-5560. https://doi.org/10.1002/2014JA019903

[27] Agapitov, O.V., Artemyev, A.V., Mourenas, D., Mozer, F.S. and Krasnoselskikh, V. (2015) *Geophysical Research Letters*, **42**, 10140-10149. https://doi.org/10.1002/2015GL066887

[28] Li, W., Mourenas, D., Artemyev, A.V., Bortnik, J., Thorne, R.M., Kletzing, C.A., *et al*. (2016) *Geophysical Research Letters*, **43**, 8867-8875. https://doi.org/10.1002/2016GL070386

[29] Chen, R., Gao, X., Lu, Q. and Wang, S. (2019) *Geophysical Research Letters*, **46**, 11671-11678. https://doi.org/10.1029/2019GL085108

[30] Artemyev, A.V. and Mourenas, D. (2020) *Journal of Geophysical Research*: *Space Physics*, **125**, e2019JA027735. https://doi.org/10.1029/2019JA027735

[31] Agapitov, O.V., Mourenas, D., Artemyev, A.V. and Mozer, F.S. (2016) *Geophysical Research Letters*, **43**, 11112-11120. https://doi.org/10.1002/2016GL071250

[32] Chen, H., Sauer, K., Lu, Q., Gao, X. and Wang, S. (2020) *AIP Advances*, **10**, Article ID: 125010. https://doi.org/10.1063/5.0026220

[33] Fan, K., Gao, X., Lu, Q., Guo, J. and Wang, S. (2019) *Journal of Geophysical Research*: *Space Physics*, **124**, 5234-5245. https://doi.org/10.1029/2019JA026463

[34] Hashimoto, K. and Matsumoto, H. (1976) *The Physics of Fluids*, **19**, 1507-1512. https://doi.org/10.1063/1.861342

[35] Stenzel, R.L. (1977) *Physical Review Letters*, **38**, 394-397. https://doi.org/10.1103/PhysRevLett.38.394

[36] Reeves, G.D., Banks, P.M., Neubert, T., Harker, K.J., Gurnett, D.A. and Raitt, W.J. (1990) *Journal of Geophysical Research*: *Space Physics*, **95**, 10655-10670. https://doi.org/10.1029/JA095iA07p10655

[37] Neubert, T. and Banks, P. (1992) *Planetary and Space Science*, **40**, 153-183. https://doi.org/10.1016/0032-0633(92)90055-S

[38] Wong, H.K. and Lin, C.S. (1990) *Radio Science*, **25**, 277-285. https://doi.org/10.1029/RS025i003p00277

[39] Nishikawa, K.-I., Frank, L.A. and Huang, C.Y. (1989) *Journal of Geophysical Research*: *Space Physics*, **91**, 6855-6865. https://doi.org/10.1029/JA094iA06p06855

[40] Sauer, K. and Sydora, R.D. (2010) *Annales Geophysicae*, **28**, 1317-1325. https://doi.org/10.5194/angeo-28-1317-2010

[41] Stix, T.H. (1962) The Theory of Plasma Waves. American Institute of Physics, New York.

[42] Sauer, K., Malaspina, D.M., Pulupa, M. and Salem, C.S. (2017) *Journal of Geophysical Research*: *Space Physics*, **122**, 7005-7020. https://doi.org/10.1002/2017JA024258

[43] Sauer, K., Baumgärtel, K., Sydora, R. And Winterhalter, D. (2019) *Journal of Geophysical Research: Space Physics*, **124**, 68-89. https://doi.org/10.1029/2018JA025887

[44] Kurita, S., Misawa, H., Cully, C.M., Le Contel, O. and Angelopoulos, V. (2012) *Geophysical Research Letters*, **39**, Article ID: L22102. https://doi.org/10.1029/2012GL053929

[45] Gendrin, R. (1961) *Planetary and Space Science*, **5**, 274-278, IN1-IN2, 279-282. https://doi.org/10.1016/0032-0633(61)90096-4

[46] Kurita, S., Katoh, Y., Omura, Y., Angelopoulos, V., Cully, C.M., Le Contel, O. and Misawa, H. (2012) *Journal of Geophysical Research*: *Space Physics*, **117**, Article ID: A11223. https://doi.org/10.1029/2012JA018076

[47] Li, W., Bortnik, J., Thorne, R.M., Cully, C.M., Chen, L., Angelopoulos, V., Nishimura, Y., Tao, J.B., Bonnell, J.W. and LeContel, O. (2013) *Journal of Geophysical Research*: *Space Physics*, **118**, 1461-1471. https://doi.org/10.1002/jgra.50176

[48] Yue, C., An, X., Bortnik, J., Ma, Q.L., Li, W., Thorne, R.M., Reeves, G.D., Gkioulidou, M., Mitchell, D.G. and Kletzing, C.A. (2016) *Geophysical Research Letters*, **43**, 7804-7812. https://doi.org/10.1002/2016GL070084

[49] Mourenas, D., Artemyev, A.V., Agapitov, O.V., Krasnoselskikh, V. and Mozer, F.S. (2015) *Journal of Geophysical Research*: *Space Physics*, **120**, 3665-3683. https://doi.org/10.1002/2015JA021135

[50] Artemyev, A., Agapitov, O., Mourenas, D., Krasnoselskikh, V., Shastun, V. and Mozer, F. (2016) *Space Science Reviews*, **200**, 261-355. https://doi.org/10.1007/s11214-016-0252-5

[51] Ma, Q., Artemyev, A.V., Mourenas, D., Li, W., Thorne, R.M., Kletzing, C.A., *et al.* (2017) *Geophysical Research Letters*, **44**, 12057-12066. https://doi.org/10.1002/2017GL075892

[52] Burton, R.K. and Holzer, R.E. (1974) *Journal of Geophysical Research*, **79**, 1014-1023. https://doi.org/10.1029/JA079i007p01014

[53] Santolík, O., Gurnett, D.A., Pickett, J.S., Parrot, M. and Cornilleau-Wehrlin, N. (2003) *Journal of Geophysical Research*: *Space Physics*, **108**, Article No. 1278. https://doi.org/10.1029/2002JA009791

[54] Li, W., Thorne, R.M., Bortnik, J., Shprits, Y.Y., Nishimura, Y., Angelopoulos, V., Chaston, C., Le Contel, O. and Bonnell, J.W. (2011) *Geophysical Research Letters*, **38**, Article ID: L14103. https://doi.org/10.1029/2011GL047925

[55] Tsurutani, B.T., Chen, R., Gao, X., Lu, Q., Pickett, J.S., Lakhina, G.S., *et al.* (2020) *Journal of Geophysical Research*: *Space Physics*, **125**, e2020JA028090. https://doi.org/10.1029/2020JA028090

[56] Dubinin, E.M., Maksimovic, M., Cornilleau-Wehrlin, N., Fontaine, D., Travnicek, P., Mangeney, A., Alexandrova, O., Sauer, K., Fraenz, M., Dandouras, I., Lucek, E., Fazakerley, A., Balogh, A. and Andre, M. (2007) *Annales Geophysicae*, **25**, 303-315. https://doi.org/10.5194/angeo-25-303-2007

[57] Tsurutani, B.T., Verkhoglyadova, O.P., Lakhina, G.S. and Yagitani, S. (2009) *Journal of Geophysical Research*: *Space Physics*, **114**, Article ID: A03207. https://doi.org/10.1029/2008JA013353

[58] Santolík, O., Kletzing, C.A., Kurth, W.S., Hospodarsky, G.B. and Bounds, S.R. (2014) *Geophysical Research Letters*, **41**, 293-299. https://doi.org/10.1002/2013GL058889

[59] Zhang, X.-J., Mourenas, D., Artemyev, A.V., Angelopoulos, V., Kurth, W.S., Kletzing, C.A. and Hospodarsky, G.B. (2020) *Geophysical Research Letters*, **47**,

e2020GL088853. https://doi.org/10.1029/2020GL088853

[60] Zhang, X.J., Agapitov, O., Artemyev, A.V., Mourenas, D., Angelopoulos, V., Kurth, W.S., *et al.* (2020) *Geophysical Research Letters*, **47**, e2020GL089807. https://doi.org/10.1029/2020GL089807

[61] Sauer, K., Dubinin, E. and McKenzie, J.F. (2002) *Geophysical Research Letters*, **29**, Article No. 2226. https://doi.org/10.1029/2002GL015771

[62] Dubinin, E.M., Sauer, K. and McKenzie, J.F. (2003) *Journal of Plasma Physics*, **69**, 305-330. https://doi.org/10.1017/S0022377803002319

[63] Katoh, Y. and Omura, Y. (2016) *Earth, Planets, and Space*, **68**, Article No. 192. https://doi.org/10.1186/s40623-016-0568-0

[64] Chirikov, B.V. (1979) *Physics Reports*, **52**, 263-379. https://doi.org/10.1016/0370-1573(79)90023-1

[65] Nunn, D., Zhang, X.-J., Mourenas, D. and Artemyev, A.V. (2021) *Geophysical Research Letters*, **48**, e2020GL092178. https://doi.org/10.1029/2020GL092178

[66] Zhang, X.-J., Demekhov, A.G., Katoh, Y., Nunn, D., Tao, X., Mourenas, D., *et al.* (2021) *Journal of Geophysical Research: Space Physics*, **126**, e2021JA029330. https://doi.org/10.1029/2021JA029330

[67] Demekhov, A.G. and Trakhtengerts, V.Y. (2008) *Radiophysics and Quantum Electronics*, **51**, 880-889. https://doi.org/10.1007/s11141-009-9093-3